SAND2022-10764J

Propellants, Explosives, Pyrotechnics

Full Paper—Original Submission

DOI: 10.1002/prep.2022#####

A liquid stratification model to predict failure in thermally damaged EBW detonators

Michael L. Hobbs*[a] and Stephanie A. Coronel[b]

Abstract: In previous work, commercially available downward facing exploding bridgewire detonators (EBWs) were exposed to elevated temperatures. These detonators were then initiated using a firing set which discharged a high amplitude short duration electrical pulse into a thin gold bridgewire. Responses of the detonators were measured using photonic doppler velocimetry (PDV) and high-speed photography. A time delay of 2 μs between EBW initiation and first movement of an output flyer separated operable detonators from inoperable detonators or duds. In the current work, we propose a simple method to determine detonator operability from the calculated state of the detonator at the time the firing set is initiated. The failure criterion is based on the gap distance between the exploding bridgewire (EBW) and the adjacent initiating explosive within the detonator which is low-density pentaerythritol tetranitrate (PETN) that melts between 413-415 K (140-142 ºC). The gap forms as PETN melts and flows to the bottom of the input pellet. Melting of PETN is modeled thermodynamically as an energy sink using a normal distribution spread over a temperature range between the onset temperature of 413 K and the ending temperature of 415 K. The extent of the melt is determined from the average temperature of the PETN. The PETN liquid is assumed to occupy the interstitial gas volume in the lower part of the input pellet. The vacated volume from the relocated liquid forms the gap between the EBW and the PETN. The remaining sandwiched layer consists of solid PETN particles and gas filling interstitial volume. We predict that a threshold gap between 17-27 μm separates properly functioning detonators from duds.

Keywords: PETN, cookoff, detonators, thermal damage

1 Introduction

The operability of an exploding bridgewire (EBW) detonator is defined as the ability of the initial pressing (IP), in contact with the EBW, to promptly shock initiate the output pellet (OP) after energy is delivered to the bridgewire that is commonly made from gold [1]. Joule heating causes the thin gold wire to rapidly melt, expand, and form an expanding plasma that subsequently collapses inward by magnetic forces [2]. This plasma can reach temperatures higher than 10,000 K and delivers thermal energy and a non-sustained shock to the IP [3].

The exploding bridgewire does not cause a prompt detonation in the IP. In fact, Smilowitz et al. [4] using modern diagnostics such as visible light emission, x-ray transmission, proton radiography, and temperature measurements, observed a delay between vaporization and detonation formation during detonator function of a custom-made (stainless-steel casing replaced with transparent casing) Teledyne RISI RP-80 detonator. The delay has been described as excess transit or lost time [5] with a detonation kernel eventually forming 1 mm from the bridgewire [4]. Even with such illuminating experimental observations, the precise mechanism of initiation in the IP remains a major unsolved problem. Rae and Rettinger [6] also measured the effects of air gaps placed intentionally between the bridgewire initiating explosive for room temperature EBWs and found that these detonators required higher voltage to

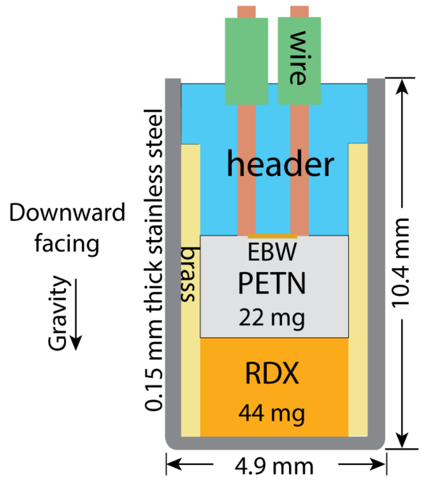

Figure 1. Schematic of a downward facing RP-87 detonator

initiate. An overview of EBW functionality in pristine detonators can be found in [7]-[9].

The present work expands our understanding of detonator functionality in accidents involving high temperatures such as fires; specifically, in detonators that contain pentaerythritol tetranitrate (PETN) [10,11]. Manner et al. [12] observed PETN melting in EBW detonators (with transparent sleeves) heated just above the melt temperature and held at those conditions for times ranging from 5-10 minutes. The detonators were positioned at various orientations with respect to gravity. Manner et al. observed that not all EBWs functioned properly. For example, the downward facing detonators and sideward facing detonators failed to initiate the OP. However, the upward facing detonators seemed to initiate the IP but the OP showed reduced performance due to a gap forming between the IP and OP. We have

[a] *Sandia National Laboratories*, Albuquerque, NM USA
**e-mail: mlhobbs@sandia.gov*

[b] *Terraform Industries*, Los Angeles, CA USA

observed that not all EBW detonators heated in the downward facing orientation fail to initiate. Downward facing detonators that have only been in the melting regime for 45 seconds or less can initiate the IP with full performance [11].

In the current study, we present a simple model to predict detonator failure in downward facing detonators by determining the gap distance between the EBW and the IP. We also present a thermal analysis of the detonator to predict temperatures, gas volume fraction, and thermal ignition. The model results are used to predict detonator failure of Teledyne RISI RP-87 EBW detonators. This detonator is shown in Fig. 1 and consists of a thin gold wire EBW. The EBW contacts an IP consisting of 22 mg of low-density PETN at 0.9 g/cm^3 and the OP consists of 44 mg RDX with a binder [13].

2 Analysis of RP-87 detonators

We recently published [14] a decomposition model of PETN that describes PETN as it transforms from the α (PETN-I) to the β (PETN-II) polymorph, melts, boils, and finally thermally ignites. This model has been applied in the current work to the RP-87 detonator in three-dimensions by using SIERRA-ARIA, a three-dimensional finite element model [15]. The decomposition model form and PETN parameters are available in [14]. RDX was modeled using a similar decomposition model described in [16]. The inert materials (stainless steel, brass sleeve, copper wires, and header) were modeled using common values for density and thermal diffusivity.

The RP-87 model includes both chemistry and mechanics to describe the evolving void structure within the thermally expanding PETN. We used a MicroMechanics Pressurization (MMP) model [17] to describes the evolving porosity in the decomposing PETN. This model predicts how decomposition gases accumulate in defects within the initial PETN. The initial distance between these defects was assumed to be 100 μm which is about half the value used in [17] for a different explosive.

The MMP model is an analytical solution of the spherically elastic mechanics equations coupled to thermally decomposing materials. The MMP model includes volumetric thermal strain and internal pressurization using well-known solutions of elastic equations that account for displacement of the condensed phase. The model also includes strain caused by decomposition.

Although the MMP model form is given in [17], the mechanics parameters for PETN were taken from [18] with a crystal density of 1.78 g/cm^3, longitudinal sound speed of 2980 m/s, shear sound speed of 1640 m/s, Poisson's ratio of 0.28, Young's modulus of 1.23×10^{10} Pa, and bulk modulus of 9.42×10^{10} Pa. The average volumetric thermal expansion coefficient of 0.000274 K^{-1} was determined for PETN using data in [19]. The density of both the solid and liquid PETN were assumed to be the same with similar volumetric expansion coefficients.

Subsection 2.1 presents various thermal predictions for the RP-87 detonators. Subsection 2.2 presents temperature and gas fraction evolution for the PETN input pellet. The observations in these two subsections are then used in section 3 to describe the failure mechanism for downward facing RP-87 detonators. The failure mechanism is based on the gap that forms between the EBW and the PETN.

2.1 Thermal predictions

Figure 2 shows a cutaway view of the RP-87 geometry and mesh used in the 3D simulations. The mesh is only shown in the IP for clarity. The complete grid converged mesh required over 180,000 hexahedral elements.

Figure 3(a) shows the ability of the 3D finite element model [14,15] to predict the time to thermal ignition when the external temperatures of the detonators were ramped at various rates. Uncertainties in these predictions were addressed in [14] and were generally within 1% of the measurements. Figure 3(b) presents the temperatures in the center plane of the detonator after heating from room temperature at 5 K/min for 1440 s. At this time, about 80 vol% of the PETN has melted, and the average temperature of the PETN IP was 414.3 K.

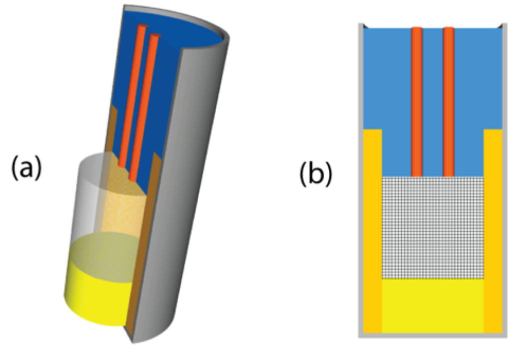

Fig. 2. (a) Cutaway view of RP-87 and (b) cross-sectional cut showing mesh in PETN

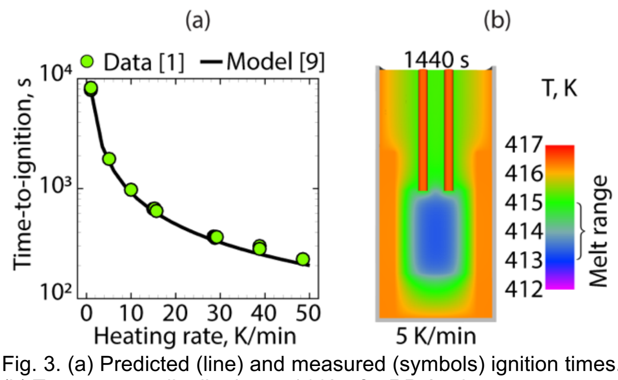

Fig. 3. (a) Predicted (line) and measured (symbols) ignition times. (b) Temperature distribution at 1440 s for RP-87 detonator ramped at 5 K/s

2.2 Mechanics

The MMP model predicts the pressure, specific surface area, and gas volume fraction within the PETN. Figure 4 shows the temporal evolution of radial temperature and gas volume. Because the PETN volume is small, the temperature rises uniformly until the PETN melts and ignites.

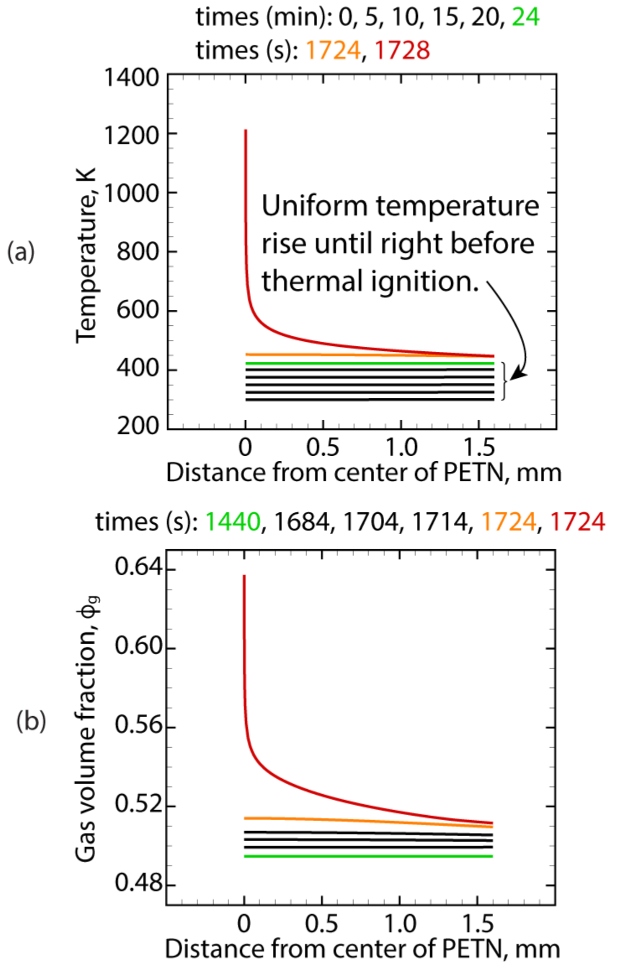

Fig. 4. (a) Predicted temperatures and (b) gas volume fraction for RP-87 detonator ramped at 5 K/s. The green line is at 1440 s which corresponds to Fig. 3(b).

We found that if the temperature of the PETN in the downward facing RP-87 detonator exceeds 414 K for more than 45 s, the detonator fails [11]. We have also found that if the PETN temperature is less than 406 K for no more than an hour, the detonator functions like a pristine detonator. Thus, the temperatures of most interest are greater than 406 K and temperatures that have been at or above 414 K for 45 seconds or less. Section 3 presents the failure model for downward facing RP-87 EBWs that depends on the gas volume fraction and the degree of melting between 413 K and 415 K.

3 Failure model for downward facing EBWs

A liquid stratification (LS) model is presented in this section. For downward facing RP-87 EBW detonators, the LS model is a subgrid model that determines the gap between the EBW and the PETN input pellet. The primary assumption of the LS model is that the liquid PETN flows to the bottom of the input pellet and fills the available gas volume with liquid PETN. For the upward facing and downward facing detonators, the gravity vector is orthogonal to the bridge wire but in opposite directions.

Average quantities are used for the volume fractions. Likewise, the average melt fraction is determined from the average temperature of the IP. The gas, liquid, and solid volume within the IP do not change during the stratification calculation. Rather, the three volumes (solid, liquid, and gas) are redistributed within the original PETN IP volume to a fill volume (AF), porous volume (AP), and a gap volume (AG) as shown in Fig. 5 with A representing the cross-sectional area of the input pellet.

For downward facing detonators, gaps form between the bridgewire and the PETN. For upward facing detonators, gaps form between the PETN and RDX. The gap is formed from the vacated volume as the liquid fills the bottom of the IP. The remaining sandwiched layer is a permeable layer that consists of solid PETN particles and gas filling the interstitial volume.

For the sideways orientation, the equations are different since the cross-sectional area is variable and not constant. For this case, the operability of the detonators depends on how much of the EBW is in contact with the PETN IP as well as the stratification of liquid PETN.

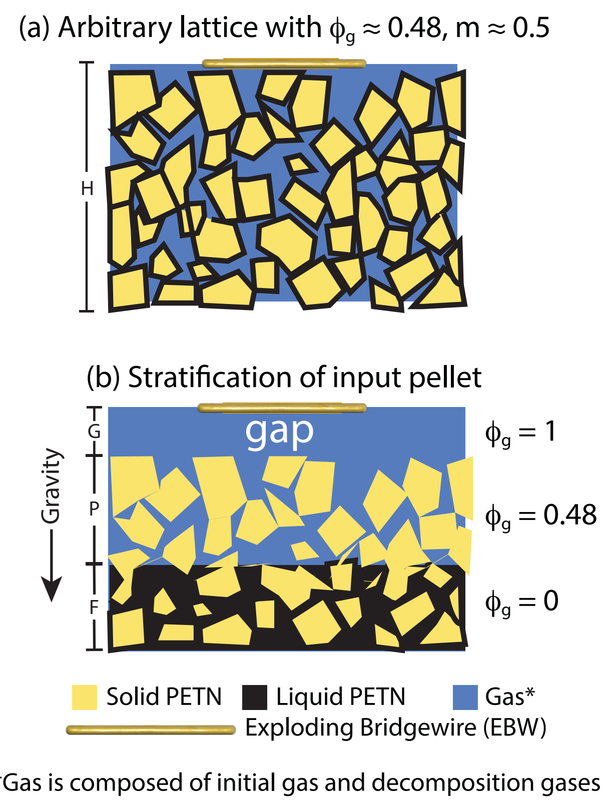

Fig. 5. (a) Initial lattice and (b) stratified lattice of IP. The model does not make any assumptions regarding particle packing.

3.1 Equations

Table 1 provides the nomenclature that is used for the derivation of the equations that define three distinct stratifications of the downward facing PETN input pellet, starting at the PETN/RDX interface: 1) liquid-solid fill region height, F, 2) solid-gas permeable region height, P, and 3) the gap between the EBW and the PETN, G. From Table 1, the overall volume fraction balance is

$$1 = \tilde{\phi}_G + \tilde{\phi}_C \text{ or} \tag{1}$$

$$\tilde{\phi}_C = 1 - \tilde{\phi}_G \tag{2}$$

where the gas volume fraction, $\tilde{\phi}_G$, includes the initial gas volume as well as gas volume created via reaction. More discussion on the gas volume fraction is given in [17].

Table 1. Nomenclature and definitions.

Symbol	Description
A	Cross-sectional area of IP (constant, pr^2)
F	Liquid-solid fill height
G	Gap height
H	Input pellet height (3.2 mm)
$\tilde{m}$	Avg. melt fraction (ranges from 0 to 1)
P	Solid-gas permeable region height
$\tilde{\phi}_C$	Avg. condensed volume fraction, $(1 - \tilde{\phi}_G)$
$\tilde{\phi}_G$	Avg. gas volume fraction
$\tilde{\phi}_L$	Avg. liquid volume fraction, $\tilde{m}(1 - \tilde{\phi}_G)$
$\tilde{\phi}_S$	Avg. solid vol. fraction, $(1 - \tilde{m})(1 - \tilde{\phi}_G)$

The condensed volume fraction, $\tilde{\phi}_C$, is composed of both the liquid PETN and solid PETN:

$$\tilde{\phi}_C = \tilde{\phi}_L + \tilde{\phi}_S, \text{ where} \tag{3}$$

$$\tilde{\phi}_L = \tilde{m}(\tilde{\phi}_C) \text{ and} \tag{4}$$

$$\tilde{\phi}_S = (1 - \tilde{m})(\tilde{\phi}_C). \tag{5}$$

The overall volume balance is then

$$1 = \tilde{\phi}_G + \tilde{m}(\tilde{\phi}_C) + (1 - \tilde{m})(\tilde{\phi}_C). \tag{6}$$

where $\tilde{m}$ represents the melt fraction discussed later in this section.

The fill volume (AF) in the LS model contains all the liquid in the PETN input pellet as well as the solid fraction that resides in the input pellet:

$$AF \equiv AH\tilde{\phi}_L + AF\tilde{\phi}_S \, . \tag{7}$$

One implicit assumption regarding Eq. (7) is that the solid volume fraction in the porous volume is the same as the average solid volume fraction within the input pellet. This is an exceptionally good assumption for the small RP-87 detonators. The small size of the input pellets results in spatially uniform temperature until just before ignition, as shown in Fig. 4. The uniform solid volume fraction assumption is not as good when the detonator thermally ignites. However, by this time, the PETN is usually liquid, and the gap distance is the gas volume fraction.

Rearrangement of Eq. (7) leads to an expression for the fractional height of the fill region (F/H):

$$F = H\tilde{\phi}_L + F\tilde{\phi}_S \tag{8}$$

$$F/H = \tilde{\phi}_L/(1 - \tilde{\phi}_S) \tag{9}$$

$$F/H = \tilde{m}(1 - \tilde{\phi}_G)/[\tilde{m} + \tilde{\phi}_G(1 - \tilde{m})] \tag{10}$$

The gap volume is based on the drained or displaced liquid volume from regions G and P which we assume happens quickly. The overall liquid volume in the input pellet is, $AH\tilde{\phi}_L$. Not all this liquid ($AH\tilde{\phi}_L$) gets displaced to region F since region F has preexisting liquid of volume $AF\tilde{\phi}_L$. In other words, only the liquid from the G and P regions can be added to the F region during stratification. Thus, the displaced liquid is the overall liquid volume minus the preexisting liquid in the F region as shown in Eq. (11):

$$AG = A(H - F)\, \tilde{\phi}_L \tag{11}$$

$$G/H = \begin{cases} (1 - F/H)[\tilde{m}(1 - \tilde{\phi}_G)] & \tilde{m} < 1 \\ \tilde{\phi}_G & \tilde{m} = 1 \end{cases} \tag{12}$$

The porous fill height (P/H) is obtained using an overall volume balance.

$$P/H \equiv 1 - F/H - G/H. \tag{13}$$

The volume fractions listed in Table 1 are functions of both the average gas volume fraction and the melt fraction. The gas volume fraction evolves based on the decomposition model [14] and pore mechanics model [17]. The average gas volume fraction is calculated by integrating ϕ_G, which is a field variable representing the spatially dependent gas volume fraction in the MMP model [17], over the IP volume and normalizing by the IP volume ($\int dV$):

$$\tilde{\phi}_G = \int \phi_G dV / \int dV \tag{14}$$

Melting was modeled thermodynamically [11] using a normal distribution spread over a range defined by 413 K and 415 K, with a mean melting temperature of 414 K. The standard deviation of the melting temperature was therefore taken to be (414 – 413)/3, or 0.333 K. The standard Z score is the number of standard deviations between the average temperature ($\tilde{T} = \int \phi_G T dV / \int \phi_G dV$) and the mean melting temperature, $Z = (\tilde{T} - 414)/0.333$. The average melt fraction in Table 1 is then determined from the normal cumulative distribution function as follows:

$$\tilde{m} = \int_{-\infty}^{z} \frac{1}{\sqrt{2\pi}} e^{-\frac{z^2}{2}} \mathrm{d}z \, . \tag{15}$$

Figure 6 shows the non-linear behavior of the fractional heights of the IP (G/H, P/H, and F/H) as the average gas volume fraction ($\tilde{\phi}_G$) ranges from 0 to 1. Each of the lines in Fig. 6 represent different average melt fractions ($\tilde{m}$). During cookoff, not all states shown in Fig. 6 are attainable since the ignition kernel is small and the average gas volume fraction does not change appreciably, e.g., see Fig. 4(b).

The width of the gray vertical line in Fig. 6 represents the expected range for RP-87 EBWs starting at the initial gas volume fraction of 0.49 and ending with an average gas volume fraction of 0.52. These values were taken from the simulation shown in Fig. 4(b) when the RP-87 was ramped at 5 K/min.

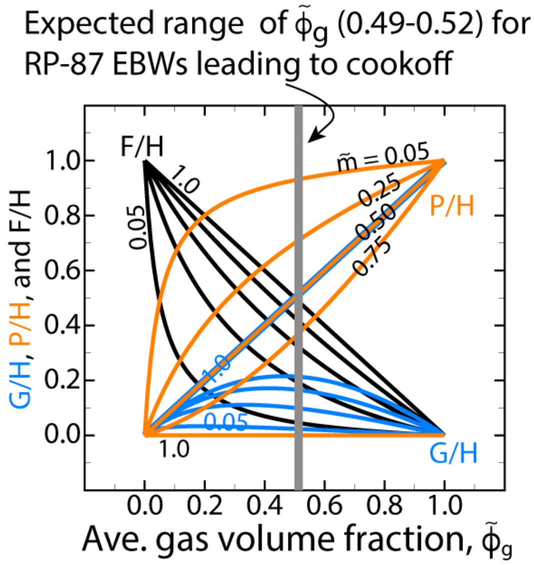

Fig. 6. Fractional IP heights as a function of $\tilde{m}$ and $\tilde{\phi}_G$.

3.2 Application to RP-87 EBWs

Coronel and Kaneshige [10] ramp heated downward facing RP-87 detonators in a 2.54 diameter hollow aluminum cylinder as shown in Fig. 7(a). Heater bands were used to heat the aluminum at 24.4±1.5 K/min to various set point temperatures (T_{SP}) in about 300 s and held until the EBW was initiated with a Reynolds FS-14 firing set. The discharge capacitor voltage (~4800 V) was nominally the same for each experiment. The total energy delivered to the EBW was about 12 J. Measured temperatures for each of the tests are shown in Fig. 7(b) where red lines represent functional detonators and green lines represent inoperable detonators.

Operability refers to whether the detonator functions as intended even when exposed to high temperatures. Operability of the RP-87 detonators was evaluated using two methods. The first method of determining operability involved high speed imaging at 1000 kfps using exposure times of 261 ns. Pristine detonators and functioning heated detonators had fast-moving luminous fronts. Nonoperational detonators had slow-moving luminous fronts. Operability was also determined using photon doppler velocimetry (PDV) to measure the function time of the RP-87 detonators. Function time is defined as the time when the EBW is actuated until first motion of the output pellet is measured with PDV. We assume that the RP-87 detonator is fully operational if the function time is comparable to the function time specified by the manufacturer.

The RP-87 detonator has a documented function time of 1.95±0.13 μs with the uncertainty represented as 1 standard deviation [13]. For pristine RP-87 detonators we measured a function time of 1.6-1.9 μs by assuming a 2 μs capacitor delay time. We also measured a function time of 1.7-2.0 μs for heated RP-87 detonators that were functional. In contrast, heated EBWs that were nonfunctional had a time delay ranging from 4.48-8.84 μs.

Table 2 presents the operability tests from [10] and includes the fractional heights (*G*/*H*, *P*/*H*, and *F*/*H*) at the time of initiation. The experiments are organized first by the time that the detonator temperature exceeded 414 K (mean melting point) and then by the firing times. In Table 2, experiments 1-14 have the same thermal profile but with longer hold times at the set point temperatures between 412.69 K and 413.16 K. The horizontal line between experiments 9 and 10 separates the functional EBWs from the non-functional EBWs. The value of *G*/*H* for experiments 9 and 10 are 0.0054 and 0.0084. The IP pellet is a 3.2 mm diameter by 3.2 mm high cylinder. As such, the gap distances at the time of initiation for functional experiment 9 and nonfunctional experiment 10 are 17 μm and 27 μm, respectively.

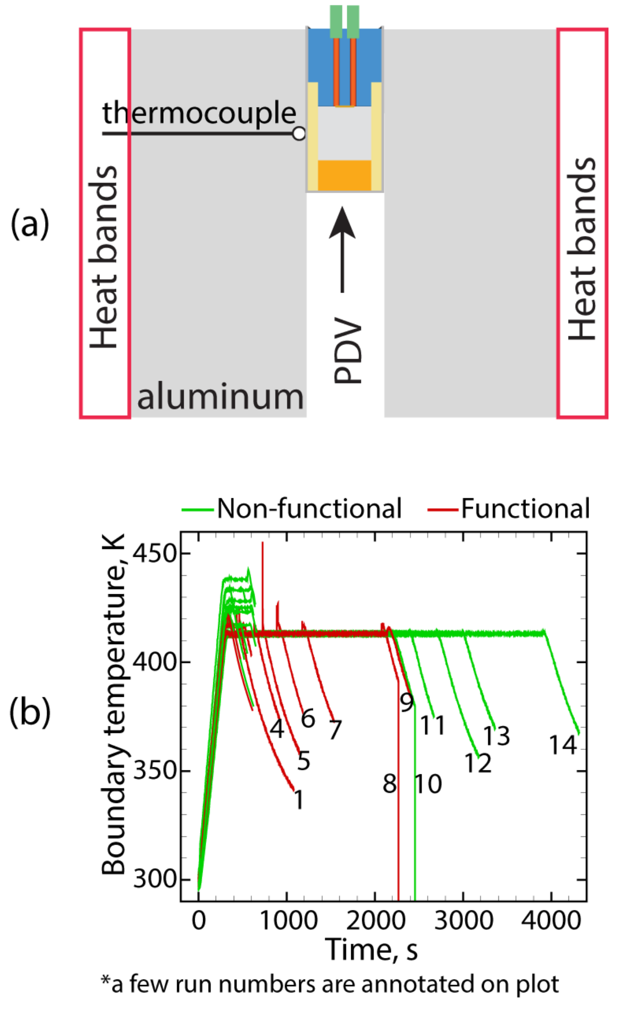

Fig. 7. (a) Test apparatus and (b) measured temperatures for RP-87 tests [10].

The horizontal line between experiments 14 and 15 separates experiments where the set point temperature is at the onset of melting (experiment 14) and fully melted (experiments 15). Notice that experiments 15-19 are fully functional even though the calculated gap is 0.8 mm (0.25×3.2 mm). The calculated gaps were determined using a thermodynamic model for the melting which is heat transfer limited.

Functioning downward facing EBWs with average temperatures calculated to be above the average melt temperature (414 K) were only at these temperatures for 33 seconds or less. The gap distance for these detonators is likely much less than the simple model predictions of 0.8 mm and illustrates a kinetic delay which may be caused by the stratifying flow.

Another issue with the failure model is that it uses the average temperature of the PETN IP, which may have temperature gradients, and the average temperature may not be the best to use to determine the stratification. For example, Fig. 8 shows the temperatures in the RP-87 for experiment 15. The average temperature in the IP is 416.8 K at the initiation time (305 s) indicating that the PETN was completely melted. However, there is a “mush zone” bounded by the grey contour line in Fig. 8 that may be responsible for the functionality of the detonator that was not predicted by the simple stratification model.

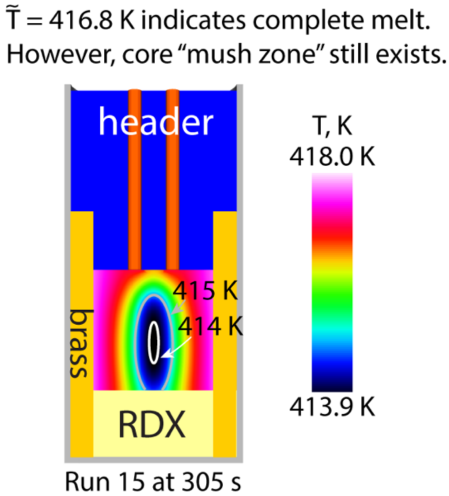

Fig. 8. Temperature distribution at 305 s for experiment 15.

Table 2. RP-87 operability data for EBWs ramped (24.4±1.5 K/min) from 299±1.6 K to various set point temperatures, (T_{SP}) in about 300 s and held until the EBW was initiated (fired) with the Reynolds FS-14 fireset.

Run	Test	T_{SP}, K	Fire t, s	t^a μs	Operable	t_{414}^b, s	T_{ave}	$\tilde{\phi}_G$	$\tilde{m}$	F/H	P/H	G/H
1	39	412.8	434.00	NA	Y	0	412.69	0.4947	0.0002	0.0000	0.9999	0.0000
2	41	412.8	463.50	NA	Y	0	413.04	0.4947	0.0020	0.0021	0.9969	0.0010
3	40	412.7	501.01	NA	Y	0	413.03	0.4947	0.0018	0.0018	0.9973	0.0009
4	42	412.9	630.50	NA	Y	0	413.12	0.4948	0.0042	0.0042	0.9937	0.0021
5	43	413.2	726.60	NA	Y	0	413.19	0.4948	0.0073	0.0074	0.9889	0.0037
6	44	412.9	887.10	NA	Y	0	413.20	0.4949	0.0079	0.0080	0.9880	0.0040
7	45	413.1	1174.15	NA	Y	0	413.17	0.4952	0.0063	0.0064	0.9904	0.0032
8	47	413.1	2074.30	NA	Y	0	413.15	0.4974	0.0056	0.0056	0.9916	0.0028
9	52	413.1	2140.35	NA	Y	0	413.23	0.4979	0.0108	0.0108	0.9839	0.0054
10	51	413.1	2191.90	NA	N	0	413.29	0.4982	0.0171	0.0169	0.9747	0.0084
11	50	413.1	2381.90	NA	N	0	413.31	0.4997	0.0197	0.0193	0.9710	0.0097
12	49	413.1	2689.47	NA	N	0	413.35	0.5025	0.0259	0.0250	0.9624	0.0126
13	48	413.1	2984.50	NA	N	0	413.46	0.5087	0.0533	0.0490	0.9261	0.0249
14	46	413.1	3900.46	NA	N	0	418.09	0.6123	1.0000	0.3877	0.0000	0.6123
15	66	417.7	305.00	1.88	Y	28	416.59	0.4947	1.0000	0.5053	0.0000	0.4947
16	71	416.6	315.00	1.83	Y	28	415.27	0.4947	1.0000	0.5053	0.0000	0.4947
17	70	418.3	305.00	1.95	Y	30	416.82	0.4947	1.0000	0.5053	0.0000	0.4947
18	74	415.7	325.00	1.92	Y	31	414.49	0.4947	0.9310	0.4875	0.2714	0.2411
19	69	418.9	305.00	NA	Y	33	417.76	0.4947	1.0000	0.5053	0.0000	0.4947
20	73	418.2	335.00	2.48	N	51	418.26	0.4947	1.0000	0.5053	0.0000	0.4947
21	65	418.2	340.00	2.84	N	60	418.11	0.4947	1.0000	0.5053	0.0000	0.4947
22	58	433.2	350.00	NA	N	85	433.56	0.4948	1.0000	0.5052	0.0000	0.4948
23	67	418.0	369.99	3.07	N	90	417.96	0.4947	1.0000	0.5053	0.0000	0.4947
24	68	416.2	470.00	NA	N	190	416.25	0.4947	1.0000	0.5053	0.0000	0.4947
25	57	433.2	470.00	4.32	N	210	433.45	0.4959	1.0000	0.5041	0.0000	0.4959
26	93	425.3	585.02	6.84	N	300	424.93	0.4953	1.0000	0.5047	0.0000	0.4953
27	90	423.4	590.00	6.39	N	300	423.29	0.4951	1.0000	0.5049	0.0000	0.4951
28	64	417.1	580.00	NA	N	310	417.78	0.4948	1.0000	0.5052	0.0000	0.4948
29	92	428.4	595.00	5.92	N	315	428.26	0.4960	1.0000	0.5040	0.0000	0.4960
30	56	433.2	580.00	4.79	N	325	433.41	0.4993	1.0000	0.5007	0.0000	0.4993
31	91	438.2	555.00	5.44	N	330	441.82	0.5280	1.0000	0.4720	0.0000	0.5280

[b] RP-87 function time assuming capacitor delay is 2 μs. Function time were not available (NA) for some of the runs.
[a] Time (s) above 414 K.

If we would have chosen the average temperature ($\tilde{T}$) of 414 K, then the melt fraction would have been 0.5 and the gap fractional height would have been about 0.17 or 0.5 mm, which is still a large gap. This analysis indicates that the inability of the simple stratification model to determine operability for experiments 10-14 is related to the limitations caused by hindered flow caused by surface wetting, surface tension, viscosity, particle packing, tortuosity, etc. Modeling these complexities is beyond the scope of the current work. Further information on the effects of flow can be found [20] where a PETN ignition model is described that includes the effects of fluid flow using a Boussinesq approximation. Adding flow improved the predictions of the ignition times. However, understanding flow in a packed bed is needed to explore the effect of flow on detonator operability,

4 Discussion

A simple model has been presented to predict the functionality of downward facing RP-87 detonators exposed to elevated temperatures that might occur during accidental fires. The failure of thermally damaged EBWs is based on the gap that forms between the gold bridge wire and the PETN input pellet. This gap was assumed to be created by the heat transfer limited melting of PETN. EBWs with calculated gaps less than or equal to 17 μm behaved like pristine detonators. Once the gap distance increased to 27 μm, the EBWs failed to operate.

For the most part, downward facing EBWs, heated to the melting point or higher, fail to function as pristine detonators. For the RP-87 EBWs, the gap formed between the bridgewire and IP is about 0.8 mm, and all RP-87 detonators were predicted to fail. However, there were a few experiments with detonators above the melting point that did not fail.

The inability of the failure mechanism to predict all measured downward facing RP-87 failures may be related to the flow of liquid PETN through the bed. The data indicates that this delay is kinetically limited, but relatively fast. Since the flow of liquid PETN through the bed is relatively fast, a simple method to predict failure of the RP-87 detonators is to 1) calculate the average temperature of the PETN, 2) calculate the average gas volume fraction within the PETN, 3) determine the extent of melting using the average temperature within the PETN, 4) calculate the gap distance between the EBW and PETN, 5) determine whether the gap is greater than 17-27 μm. Typically, the downward facing RP-87 will not function properly if the gap distance is above this critical range (17-27 μm). However, if the detonator has only been above the average melting temperature (414 K) for about 45 seconds or less, the detonator will be operational.

Although a 3D finite element model was used to make some of the predictions in the current work, this level of rigor is not necessary to predict detonator failure. Simpler 1D models as used in [11] are sufficient to calculate the parameters necessary to determine detonator failure.

The model equations have only been derived for the downward facing detonators. These equations are also sufficient for upward facing detonators, but the gap forms between the PETN input pellet and the RDX output pellet. In this orientation, the PETN may run to detonation, but the shock must traverse the gap making initiation of the RDX difficult. We suggest additional experiments be performed in both downward and side facing directions. Future work should also include shock physics modeling of the EBWs and include gaps between both the bridgewire and IP and the gap at the IP and OP interface. The critical gap distance (17-27 μm) for downward facing RP-87 EBWs is likely a function of 1) the capacitor discharge and the diameter of the gold bridgewire and 2) the initial density of the PETN input pellet (0.9 g/cm^3). The current work suggests that small gaps on the same order as the bridgewire diameter could be responsible for inoperability of EBW detonators. Future work should explore the effects of discharge energy and initial PETN density on EBW detonator operability. More characterization of PETN such as liquid density, viscosity, and PETN-gold wettability is also suggested. Alternate inoperability models based on local increase in density caused by liquid PETN filling void space near the bridgewire should also be considered for future work.

Acknowledgements

Sandia National Laboratories is a multimission laboratory managed and operated by National Technology & Engineering Solutions of Sandia, LLC, a wholly owned subsidiary of Honeywell International Inc., for the U.S. Department of Energy's National Nuclear Security Administration under contract DE-NA0003525. The authors acknowledge partial support of this work from the Joint DoD/DOE Munitions Program. This paper describes objective technical results and analysis. Any subjective views or opinions that might be expressed in the paper do not necessarily represent the views of the U.S. Department of Energy or the United States Government. We would like to thank Michael Kaneshige, Michael Powell, and John Niederhaus for illuminating discussions regarding EBW functionality. We would also like to thank Shane Snedigar for running the RP-87 operability experiments, Shane Schumacher, Bill Erikson, David Damm, and Dan Guildenbecher for internal review, and Jeremy Lechman and Xiaomei "Mei" Qiu for management support.

References

[1] P. J. Rae, The action-integral and energy to explode short gold wires in ambient air, *Phys. Plasmas*, **2021**, *28*, 033509. DOI: 10.1063/5.0041067.

[2] C. A. Hrousis, J. S. Christensen, Advances in Modeling Exploding Bridgewire Initiation, *14th International Detonation Symposium*, April 11-16, **2010**, Coeur d'Alene Resort, ID, USA, 1469-1476.

[3] R. Han, J. Wu, A. Qiu, W. Ding, Y. Zhang, Electrical explosions of Al, Ti, Fe, Ni, Cu, Nb, Mo, Ag, Ta, W, W-Re, Pt, and Au wires in water: a comparison study, *J. Appl. Phys.*, **2018,** 124, 43302. DOI: 10.1063/1.5030760.

[4] L. Smilowitz, B. F. Henson, D. Remelius, P. Bowlan, N. Suvorava, J. Allison, D. Cardon, M. Freeman, F. Mariam, W. Meijer, C. Morris, L. Neukirch, K. Prestridge, M. Sandstrom, A. Saunders, T. Schurman, A. Tainter, Z. Tang, F. Trouw, D. Tupa, J. Tybo, R. Uliano, Experimental observations of exploding bridgewire detonator function, *J. Appl. Phys.*, **2020**, 128, 215901.

[5] L. Smilowitz, D. Remelius, N. Suvorova, P. Bowlan, D. Oschwald, B.F. Henson, Finding the "lost-time" in detonator function, *Appl. Phys. Lett.*, **2019**, 114, 104102.

[6] P. J. Rae, R. C. Rettinger, The effects of air gaps and inert layers on exploding bridgewire detonator

function, *J. Energ. Mater.*, **2020,** 40, 34-45. DOI: 10.1080/07370652.2020. 1825545

[7] R. Varosh, Electric Detonators: EBW and EFI, *Propell. Explos. Pyrot.*, **1996,** 21, 150-154.

[8] P. W. Cooper, Chapter 25 Exploding Bridgewire Detonators in: Explosives Engineering, Wiley-VCH, New York **1996**, pp. 353-368.

[9] P. J. Rae, P. M. Dickson, A review of the mechanism by which exploding bridge-wire detonators function, P. R. Soc. A, **2019**, 475,1-22.

[10] S. A. Coronel, M. J. Kaneshige, Response of PETN detonators to elevated temperatures, *Proc. Combust. Inst.*, **2021**, 38, 4271-4279.

[11] M. L. Hobbs, M. J. Kaneshige, S. A. Coronel, Operability thresholds for thermally damaged EBW detonators, *Combust. Flame*, **2022**, 238, 111953.

[12] V. W. Manner, J. D. Yeager, L. Smilowitz, D. Remelius, B. F. Henson, Function of a PETN-based exploding bridgewire detonator post melt, *Propell. Explos. Pyrot.*, **2020**, 45, 1533-1540.

[13] Teledyne Energetics online reference (2021).https://www.teledynedefenseelectronics.com/energetics/Documents/RP-87.pdf

[14] M. L. Hobbs, M. J. Kaneshige, Transforming polymorphs, melting, and boiling during cookoff of PETN, *Combust. Flame*, **2022**, 237, 111877.

[15] Development team, SIERRA Multimechanics Module: Aria User Manual—Version 5.0, Report SAND2021-3921, Sandia National Laboratories, Albuquerque, NM, USA **2020**.

[16] M. L. Hobbs, M. J. Kaneshige, C. D. Yarrington, Large deformation and gas retention during cookoff of a plastic bonded explosive (PBX 9407), *Combust. Flame*, **2018**, 198, 278-289.

[17] M. L. Hobbs, J. A. Brown, M. J. Kaneshige, C. Aviles-Ramos, A micromechanics pressurization model for cookoff, *Propell. Explos. Pyrot.*, **2022**, 46, 1-16. doi.org/10.1002/prep.202100155.

[18] S. P. Marsh, editor, LASL shock hugoniot data, University of California Press, Berkeley, **1980**.

[19] T. R. Gibbs, A. Popolato, editors, LASL explosive property data, University of California Press, Berkeley, **1980**.

[20] M. L. Hobbs, S. A. Coronel, M. J. Kaneshige, Modeling PETN-based Detonators at Elevated Temperatures, 51th International Annual Conference of the Fraunhofer ICT, Energetic Materials – Exploring and Understanding, June 28–July 1, 2022, Karlsruhe, Germany.

Received:
Revised: